A Letters Journal Exploring the Frontiers of Physics

OFFPRINT

Holstein polaron in the presence of disorder

M. Berciu, A. S. Mishchenko and N. Nagaosa

EPL, **89** (2010) 37007

A Letters Journal Exploring the Frontiers of Physics

February 2010

EPL, **89** (2010) 37007
doi: 10.1209/0295-5075/89/37007

www.epljournal.org

Holstein polaron in the presence of disorder

M. Berciu[1], A. S. Mishchenko[2,3] and N. Nagaosa[2,4]

[1] *Department of Physics and Astronomy, University of British Columbia - Vancouver, BC, Canada, V6T 1Z1*
[2] *Cross-Correlated Materials Research Group (CMRG), ASI, RIKEN - Wako 351-0198, Japan*
[3] *Russian Research Centre "Kurchatov Institute" - 123182 Moscow, Russia*
[4] *Department of Applied Physics, University of Tokyo - 7-3-1 Hongo, Bunkyo-ku, Tokyo 113, Japan*

received 5 November 2009; accepted in final form 20 January 2010
published online 19 February 2010

PACS 71.38.-k – Polarons and electron-phonon interactions
PACS 72.10.Di – Scattering by phonons, magnons, and other nonlocalized excitations
PACS 63.20.kd – Phonon-electron interactions

Abstract – Non-local, inhomogeneous and retarded response similar to that observed in experiments is studied theoretically by introducing the Inhomogeneous Momentum Average (IMA) approximation for single-polaron problems with disorder in the on-site potential and/or spatial variations of the electron-phonon couplings and/or phonon frequencies. We show that the electron-phonon coupling gives rise to an additional inhomogeneous, strongly retarded potential. This potential describes essential physics ignored by "instanteneous" approximations. The accuracy of IMA is demonstrated by comparison with single-impurity results from the approximation-free Diagrammatic Monte Carlo (DMC) method. Its simplicity allows for easy study of many problems that were previously unaccessible.

Understanding the properties of materials which are the focus of current research, as well as the development of novel applications, is closely linked to the physics of quasi-particles (*qp*) in disordered systems and coupled to various bosonic modes. For example, the manganites which exhibit colossal magnetoresistance are doped materials [1] with considerable electron-phonon (el-ph) as well as electron-magnon and electron-orbiton couplings [2]; the interplay between disorder [3] and the coupling to bosons manifests itself in the peculiarities of their phase diagram [4]. Similarly, underdoped high-T_c cuprate superconductors are inhomogeneous materials [5] with rather strong and inhomogeneous coupling to phonons [6,7], besides strong coupling to magnons. Other examples are charge transport in organic thin-film transistors [8] and in organic photoreceptors [9], dominated by polaron jumps between potential traps [10]. The importance of the interplay between disorder and coupling to bosons is magnified by the fact that weak coupling, which is relatively unimportant in a clean system, may result in dramatic effects in disordered compounds [11–13].

The tremendous computational difficulties for studying a polaron even near a *single* impurity resulted in the 30 year delay between the first results based on the adiabatic approximation [14] and the recent approximation-free solution by the DMC method [11,12]. What is needed in practice, however, is the ability to generate accurate theoretical predictions for systems whose inhomogeneity is not limited to a single impurity but may have any spatial profile, including potential barriers to model interfaces, and also cases where the bosons' energies and their coupling to the electron are inhomogeneous as well [15]. Accurate numerical solution of such problems for large systems is still effectively impossible —while polarons in the presence of Anderson disorder have been investigated by calculating the distribution of the local density of states using statistical dynamic mean-field theory [16], this approach takes spatial correlations into account in an effective way only.

In this letter we study accurately yet efficiently the single-Holstein-polaron problem with arbitrary disorder by developing the Inhomogeneous Momentum Average (IMA) method. This is based on the Momentum Average (MA) approximation for translationally invariant systems, like Holstein [17] and more general models [18]. IMA takes any potential inhomogeneity into account *exactly* and also can handle inhomogeneities of the coupling and of the energy of the bosons. Comparing results of IMA with approximation-free data from DMC allows us to gauge its accuracy. The IMA approximation can then be systematically improved [19] so that in combination with DMC [11] one gets an accurate and fast tool to study all

the systems described above within the framework of a controllable and efficient approximation scheme.

Given the low computational cost of IMA, a rapid scan of the entire parameter space is now possible. To show its relevance for experimental data analysis, we compute STM images of inhomogeneous systems of large enough sizes to render DMC studies impractical, due to the enormous computational costs [20]. This allows us to prove the nonlocal nature of a system's response to disorder and demonstrate the importance of the retardation effects.

Consider the Holstein Hamiltonian with disorder

$$\mathcal{H} = \mathcal{H}_0 + \hat{V}_d + \hat{V}_{el-ph}, \tag{1}$$

where $\mathcal{H}_0 = \hat{T} + \Omega \sum_i b_i^\dagger b_i$ is the energy of the free electron, *e.g.* due to nearest-neighbor hopping on the lattice of interest, plus the free bosons ($\hbar = 1$). $\hat{V}_d = \sum_i \epsilon_i c_i^\dagger c_i$ is the disorder potential, and $\hat{V}_{el-ph} = g \sum_i c_i^\dagger c_i \left(b_i^\dagger + b_i\right)$ is the el-ph interaction. The electron's spin is irrelevant. For simplicity, we first take Ω and g to be spatially homogeneous and discuss generalizations later on.

The goal is to compute the retarded Green's function:

$$G_{ij}(\omega) = \langle 0|c_i \hat{G}(\omega) c_j^\dagger|0\rangle = \sum_\alpha \frac{\langle 0|c_i|\alpha\rangle\langle\alpha|c_j^\dagger|0\rangle}{\omega - E_\alpha + i\eta}, \tag{2}$$

where $\hat{G}(\omega) = [\omega - \mathcal{H} + i\eta]^{-1}$ and $\mathcal{H}|\alpha\rangle = E_\alpha|\alpha\rangle$ are the one-electron eigenstates. The local density of states (LDOS) $A(i,\omega) = -\frac{1}{\pi}\,\mathrm{Im}\, G_{ii}(\omega)$ is measured by STM.

Let $G_{ij}^{(d)}(\omega) = \langle 0|c_i \left[\omega - \mathcal{H}_d + i\eta\right]^{-1} c_j^\dagger|0\rangle$ be the "disorder" Green's function in the absence of el-ph coupling, corresponding to $\mathcal{H}_d = \mathcal{H}|_{g=0}$. Since $\mathcal{H}_d$ is quadratic, it can be diagonalized and thus $G_{ij}^{(d)}(\omega)$ is straightforward to calculate and treats the on-site disorder *exactly*. The diagrammatic solution is depicted in fig. 1(a). Given that $\mathcal{H} = \mathcal{H}_d + \hat{V}_{el-ph}$, we can use the Dyson identity $\hat{G}(\omega) = \hat{G}^{(d)}(\omega) + \hat{G}(\omega)\hat{V}_{el-ph}\hat{G}^{(d)}(\omega)$ to calculate $G_{ij}(\omega)$ in terms of $G_{ij}^{(d)}(\omega)$. This leads to the equation of motion

$$G_{ij}(\omega) = G_{ij}^{(d)}(\omega) + g \sum_{j_1} F_{ij_1}^{(1)}(\omega) G_{j_1 j}^{(d)}(\omega), \tag{3}$$

where $F_{ij}^{(n)}(\omega) = \langle 0|c_i \hat{G}(\omega) c_j^\dagger b_j^{\dagger n}|0\rangle$ is a generalized propagator, with $F_{ij}^{(0)}(\omega) = G_{ij}(\omega)$. Using the Dyson identity again, we find its equation of motion for $n \geqslant 1$:

$$F_{ij}^{(n)}(\omega) = g \sum_{j_1 \neq j} G_{j_1 j}^{(d)}(\omega - n\Omega)\langle 0|c_i \hat{G}(\omega) c_{j_1}^\dagger b_{j_1}^\dagger b_j^{\dagger n}|0\rangle + g G_{jj}^{(d)}(\omega - n\Omega)\left[n F_{ij}^{(n-1)}(\omega) + F_{ij}^{(n+1)}(\omega)\right]. \tag{4}$$

In the IMA$^{(0)}$ approximation, we set in all these equations $G_{j_1 j}^{(d)}(\omega - n\Omega) \to 0$ if $j \neq j_1$ and $n > 0$. This is a good low-energy approximation, because the ground-state (GS) of the polaron lies below the spectrum of $\mathcal{H}_d$ and so for $\omega \sim E_{GS}$, $G_{ij}^{(d)}(\omega - n\Omega)$ *decreases exponentially* with the distance $|i-j|$. Thus, IMA$^{(0)}$ ignores only exponentially small contributions, while keeping the large terms fully. Its physical meaning becomes more apparent in terms of a diagrammatic expansion, which can be obtained from the equations of motion in the limit of weak coupling. (Note that the equations of motion are valid for any coupling strength, they are not perturbative.) Following arguments similar to those of ref. [19], one can show that IMA$^{(0)}$ keeps all the diagrams in the diagrammatic expansion, up to exponentially small contributions which are discarded. For example, instead of the exact expression for the diagram of fig. 1(b), namely $g^4 \sum_{n,m} G_{in}^{(d)}(\omega) G_{nm}^{(d)}(\omega - \Omega) G_{mn}^{(d)}(\omega - 2\Omega) G_{nm}^{(d)}(\omega - \Omega) G_{mj}^{(d)}(\omega)$, in IMA$^{(0)}$ we keep all $n = m$ terms but ignore the exponentially smaller $n \neq m$ terms. This holds true for all diagrams, to all orders, and it is in this sense that we claim that IMA$^{(0)}$ sums all the diagrams. This approximation can be improved systematically, just like in the bulk case [19]. In IMA$^{(1)}$, off-diagonal terms are ignored only for disorder propagators with energy $\omega - n\Omega$, where $n > 1$ (the lower the energy, the faster the exponential decay), and so on and so forth. It is also worth pointing out a variational meaning. IMA$^{(0)}$ is equivalent to working in the Hilbert subspace spanned by $c_i (b_j^\dagger)^n|0\rangle$, for all i, j, n. In IMA$^{(1)}$, one extra phonon can be present at any other site [19,21], etc.

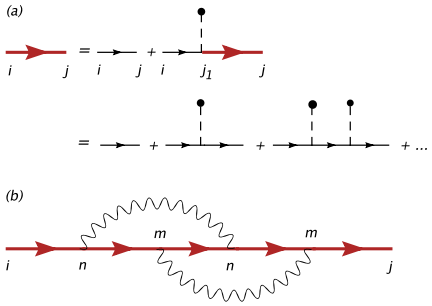

Fig. 1: (Color online) (a) The disorder Green's function (bold red line) is the usual sum of diagrams involving the free-electron propagator (thin line) and scattering on the disorder potential (dashed lines ending with circles). (b) One of the second-order diagrams contributing to the full propagator $G_{ij}(\omega)$. The wriggly lines are phonons. For more details, see text.

For both zero coupling and zero free-electron bandwidth limits, these approximations become *exact*. The arguments above explain why the low-energy part is expected to remain accurate for any intermediate coupling. Then we can use spectral-weight sum rules to gauge the accuracy of the entire spectral weight. Following the steps detailed in refs. [17,19], it is straightforward to show that IMA$^{(0)}$ obeys six spectral-weight sum rules *exactly*, while IMA$^{(1)}$ obeys eight spectral-weight sum rules *exactly*. As a result, we expect that these approximations are accurate for all couplings, at all energies, just like their bulk counterparts.

Within IMA$^{(0)}$, then, only the terms with $F^{(n)}$ functions remain in eq. (4), whose solution becomes

$F_{ij}^{(n)}(\omega) = A_n(j,\omega)F_{ij}^{(n-1)}(\omega)$ [17]. The continued fractions

$$A_n(j,\omega) = \frac{ngG_{jj}^{(d)}(\omega - n\Omega)}{1 - gG_{jj}^{(d)}(\omega - n\Omega)A_{n+1}(j,\omega)} \tag{5}$$

are easy to compute. Using $F_{ij}^{(1)}(\omega) = A_1(j,\omega)G_{ij}(\omega)$, eq. (3) becomes

$$G_{ij}(\omega) = G_{ij}^{(d)}(\omega) + g\sum_{j_1} G_{ij_1}(\omega)A_1(j_1,\omega)G_{j_1 j}^{(d)}(\omega). \tag{6}$$

This allows $G_{ij}(\omega)$ to be calculated from a system of linear equations, however the results converge extremely slowly with the cutoff in j_1. To improve efficiency, we define

$$A_n(\omega) = A_n(j,\omega)|_{\hat{V}_d=0} = A_n(j,\omega)|_{|j|\to\infty}, \tag{7}$$

i.e. $A_n(\omega)$ are the values for the clean system, familiar from MA$^{(0)}$. The second equality holds because we assume that the disordered region, however large it may be, is finite: $\epsilon_i \to 0$ when $|i| \to \infty$. Then, sites located very far from the disordered region are not sensitive to it, and propagators at such sites approach the bulk values. Introducing the "effective interaction" potential

$$v_0(j,\omega) = gA_1(j,\omega) - \Sigma_{\mathrm{MA}^{(0)}}(\omega), \tag{8}$$

where the bulk MA$^{(0)}$ self-energy is $\Sigma_{\mathrm{MA}^{(0)}}(\omega) = gA_1(\omega)$ [19], we can rewrite eq. (6) as

$$G_{ij}(\omega) = G_{ij}^{(d)}(\tilde{\omega}) + \sum_{j_1} G_{ij_1}(\omega)v_0(j_1,\omega)G_{j_1 j}^{(d)}(\tilde{\omega}), \tag{9}$$

where $\tilde{\omega} = \omega - \Sigma_{\mathrm{MA}^{(0)}}(\omega)$. This renormalized energy reveals that certain classes of diagrams have been explicitly summed (see below), and eq. (9) is now very efficient to solve numerically since $v_0(j,\omega) \to 0$ rapidly with increasing $|j|$. For a single attractive impurity $\epsilon_i = -U\delta_{i,0}$, we find that a cutoff $|j| \leqslant 5$ suffices for convergence, although a cutoff of 0 or 1 *does not*, showing that $v_0(j,\omega)$ is spread over a few sites even if the impurity is local.

Equation (9) reveals a twofold role of the el-ph interaction. The first is the renormalization $\omega \to \tilde{\omega}$. If we had found the solution $G_{ij}(\omega) = G_{ij}^{(d)}(\tilde{\omega})$, it would mean that the renormalized quasiparticle — the polaron — interacts with the disorder potential $\hat{V}_d$. However, the second term in eq. (9) shows that the disorder is renormalized as well

$$\hat{V}_d \to \hat{V}_d + \sum_j v_0(j,\omega)c_j^\dagger c_j. \tag{10}$$

In other words, due to el-ph interactions, the polaron interacts with a renormalized, retarded disorder potential.

The origin of this additional, retarded potential becomes clear if we again analyze the meaning of IMA$^{(0)}$ in terms of diagrams. As already discussed, IMA$^{(0)}$ sums *all* diagrams, such as the one depicted in fig. 1(b), except for exponentially small terms whose removal allows us to

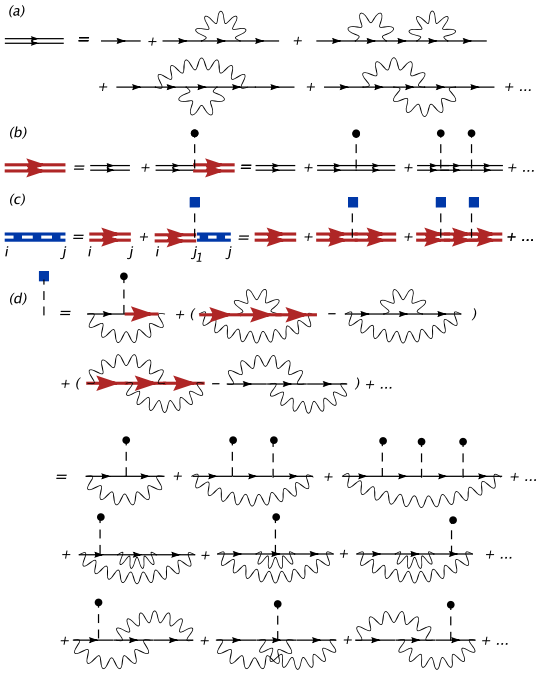

Fig. 2: (Color online) (a) The bulk polaron propagator in the clean system. MA$^{(0)}$ discards exponentially small contributions from each of these diagrams (see text for details). (b) Diagrammatic series for $G_{ij}^{(d)}(\tilde{\omega})$, which is represented by the thick red double line. Circles indicate scattering on the disorder potential. (c) Diagrammatic representation of eq. (9). The thick dashed blue line represents the full propagator $G_{ij}(\omega)$. The square box represents the additional scattering potential $v_0(j,\omega)$. (d) Diagrammatic expansion for $v_0(j,\omega)$. All phonon lines begin and end at the same site j, and each diagram contains at least one scattering on the bare disorder potential.

sum infinite classes of diagrams explicitly, in the continued fractions. However, the resulting eq. (6) cannot be summed efficiently. Unlike eq. (6), eq. (9) involves disorder propagators with the renormalized energy $G_{ij}^{(d)}(\tilde{\omega})$. These are given by a diagrammatic expansion like in fig. 1(a), but now all free electron propagators have the renormalized energy $\tilde{\omega}$, $G_0(i,j,\omega) \to G_0(i,j,\omega - \Sigma_{\mathrm{MA}^{(0)}}(\omega))$, *i.e.* they equal the bulk polaron propagator (in the absence of disorder). This propagator and its diagrams are depicted in fig. 2(a) as a double thin line. As discussed, within the MA$^{(0)}$ approximation, it equals the sum over all diagrams shown in fig. 2(a), except for exponentially small contributions which are discarded.

The diagrammatic expansion of $G_{ij}^{(d)}(\tilde{\omega})$ (denoted by a double thick line) is then shown in fig. 2(b) and should be contrasted with fig. 1(a). This figure explains our statement that $G_{ij}^{(d)}(\tilde{\omega})$ represents the bulk polaron being scattered by the *bare* disorder potential. Given that the bulk polaron diagrams all begin and end with a free-electron propagator, see fig. 2(a), it follows that $G_{ij}^{(d)}(\tilde{\omega})$ has contributions only from processes *where the electron scatters on the disorder potential when no phonons are present*. This clearly illustrates why a second term is

needed in eq. (9), to account for the processes where *the electron scatters on the disorder potential while phonons are present.*

Figure 2(c) depicts the diagrammatic analog of eq. (9), showing these extra terms which are due to scattering on the additional potential $v_0(j,\omega)$, depicted as a box (the bare potential is depicted by a filled circle, see fig. 1(a)). The diagrams contributing to $v_0(j,\omega)$ are obtained by expanding eq. (8) in powers of g; the first few terms are sketched in fig. 2(d). All phonon lines in all diagrams contributing to $v_0(j,\omega)$ start and end at site j. This is a consequence of the fact that only diagonal terms $G^{(d)}_{jj}(\omega)$ appear in the expression of $v_0(j,\omega)$, see eqs. (5) and (8). However, since $G^{(d)}_{jj}(\omega)$ is calculated exactly, these terms allow the electron to scatter on disorder at any other site in the system. This explains why $v_0(j,\omega)$ is not local, even if the bare disorder $\hat{V}_d$ is: there is a distribution of probabilities for the electron to be at various distances away from its phonon cloud, and so it can scatter on disorder potential located away from where the phonons are. Finally, the origin of the retardation effects encoded in $v_0(j,\omega)$ is now also apparent: at different energies, the structure of the phonon cloud is different, so the scattering of the electron in the presence of its cloud will be different. Typically $v_0(j,\omega)$ changes sign as ω varies, going from strongly attractive to strongly repulsive and back. Its plot for a different but related problem is shown in ref. [22].

Since $\hat{V}_d$ is treated exactly, we expect the validity of IMA$^{(0)}$ to mirror that of MA$^{(0)}$, and thus to worsen in lower dimensions d, and when the effective el-ph coupling $\lambda = g^2/(2dt\Omega) \sim 1$ (remember that IMA is exact for both $\lambda \to 0, \infty$) and for small $\Omega \to 0$ [19]. Even then, attractive potentials improve the accuracy as they push the GS to lower energies. However, for small Ω and $\lambda \sim 1$ we may need to go to a higher level of the approximation. As already explained, in IMA$^{(1)}$ we neglect the exponentially small terms in eq. (4) only if there are $n \geqslant 2$ phonons present. After long but straightforward calculations, we find that the IMA$^{(1)}$ solution is similar to eq. (9), but as expected $\tilde{\omega}$ is now renormalized by the bulk $\Sigma_{\mathrm{MA}^{(1)}}(\omega)$ self-energy [19], while the renormalized potential is also more accurate: $v_1(j,\omega) = g^2 x_{j,\omega}/[1 - g x_{j,\omega}[A_2(j,\omega) - A_1(j,\omega-\Omega)]] - \Sigma_{\mathrm{MA}^{(1)}}(\omega)$ where $x_{j,\omega} = G_{\mathrm{MA}^{(0)},jj}(\omega-\Omega)$ is the MA$^{(0)}$ solution of eq. (9) at a shifted energy. If necessary, one can go to a higher IMA$^{(n)}$ level with $n \geqslant 2$.

In fig. 3(a) we plot the LDOS $A(0,\omega)$ at the impurity site, for a single attractive impurity $\epsilon_i = -U\delta_{i,0}$ in 1D (we plot $\tanh A$ so that low-weight features are visible). At $U = 0$, it shows the expected spectrum: a narrow polaron band, a wider band for the second bound state [23], the continuum above $\omega \approx -2.5$ etc. For $U > 0$ bound states split from all the bands, redistributing the LDOS.

The accuracy of IMA is gauged against DMC results available for this single-impurity case. The GS energy and *qp* weight Z_{gs} at the impurity site *vs.* the impurity strength U is shown in figs. 3(b)–(g). The agreement is very good

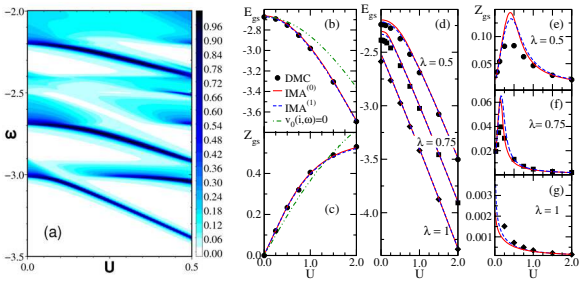

Fig. 3: (Color online) (a) $\tanh[A(0,\omega)]$ for IMA$^{(1)}$ LDOS $A(0,\omega)$ at the impurity site as a function of ω and U, for $t = 1, \Omega = 0.5, g = \sqrt{1.25}, \eta = 0.0025$; (b),(d) GS energies; and (c),(e)–(g) spectral weights Z_{gs} at the impurity site *vs.* U in DMC, IMA$^{(0)}$ and IMA$^{(1)}$, for $\Omega = 2$, $\lambda = g^2/(2t\Omega) = 0.5626$ in (b) and (c), respectively, $\Omega = 0.2$ and $\lambda = 0.5, 0.75, 1$ in (d)–(g). The dot-dashed lines in (b) and (c) show results for the case of a simple energy shift by $-g^2/\Omega$, *i.e.* for $v_0(i,\omega) = 0$.

in panels (b), (c) even though these are 1D results, where IMA is least accurate. This is partially due to the large $\Omega = 2t$ [19]. For a worst-case scenario, we plot in (d)–(g) results for a much smaller $\Omega = 0.2t$, for weak, medium and strong couplings. Here we see quantitative differences. For E_{gs}, the accuracy at small U mirrors that of MA in the bulk [19]. As noted, when U increases and E_{gs} moves to lower energies, the accuracy improves. Z_{gs} shows more significant errors at small U, with IMA overestimating the answer. This is not surprising, since for such small Ω one expects phonons at many different sites and a higher level n of IMA is needed. However, even $n = 0, 1$ levels capture the results quantitatively quite well, even in 1D. Given the 6 (8) spectral-weight sum rules satisfied exactly by IMA$^{(0)}$ (IMA$^{(1)}$), we expect the spectral weight at all energies to be similarly accurate.

Figures 3(b), (c) also show results (dash-dotted line) for the *instantaneous approximation* [24,25], where the el-ph coupling is assumed to simply shift energies by the polaron formation energy $-g^2/\Omega$. In IMA, this shift comes from $\Sigma_{\mathrm{MA}}(\omega \approx E_{\mathrm{gs}}) \approx -g^2/\Omega$ appearing in $\tilde{\omega}$, so it implies setting $v_0(j,\omega) \to 0$. In fact, using the full bulk self-energy instead of $-g^2/\Omega$ also accounts for the renormalization of the polaron mass, which is linked to the $\partial\Sigma(\omega)/\partial\omega$. Even so, this works rather poorly even for this small λ and it gets worse as either U or g increases. This demonstrates that $v_0(j,\omega)$ cannot be ignored, and that instantaneous approximations that do so are of limited accuracy. This is not surprising, given the meaning of $v_0(j,\omega)$ revealed in fig. 2. Ignoring $v_0(j,\omega)$ means that one only allows the electron to scatter when no phonons are present. However, the stronger the coupling g is, the bigger is the probability that phonons are always present, and therefore the more important the scattering of the electron *in the presence of the phonon cloud*, captured by $v_0(j,\omega)$, becomes.

This conclusion must be of much wider generality: even for interacting particles in the presence of disorder, one should expect such a renormalization of the disorder, due

to scattering of the electron on disorder in the presence of its cloud of particle-hole excitations. Ignoring this renormalization, as done by instantaneous approximations, is unjustifiable if the interactions are strong.

Note that all the analysis so far assumed homogeneous g and Ω values. Inhomogeneities in g and Ω are easy to treat with our method, since all its equations and approximations are formulated in real space. Repeating the same steps, one finds that at the IMA$^{(0)}$ level one simply has to use the appropriate g_j and Ω_j values in eqs. (5) and (8), and similar changes are needed for IMA$^{(1)}$. However, the general structure of all the equations and the computational effort required to solve them is unchanged. The extra diagrams contributing to $v_0(j,\omega)$ when g or Ω are inhomogeneous can also be identified easily. Even if there is no bare disorder, a $v_0(j,\omega)$ will appear at all sites j with a different g_j or Ω_j, to account for differences between their contributions and those of the bulk diagrams.

This shows that IMA allows us to consider all possible sources of disorder on equal footing, at no added computational cost, and that all lead to the renormalization of the bare disorder. It is true that unlike $\hat{V}_d$, inhomogeneities in g and Ω are not treated exactly. However, they are treated at the same level of accuracy as all other electron-phonon interactions, based on the same arguments of disregarding exponentially small contributions while obeying exactly multiply spectral-weight sum rules. We are thus confident that IMA maintains the level of accuracy shown in fig. 3, although lack of exact numerical results for cases with inhomogeneous g or Ω prevents us from verifying this.

Besides revealing interesting physics, as already discussed IMA allows for efficient study of large disordered samples, including their Fourier transform (FT) analysis. FT-STM, pioneered in ref. [26], is being applied not only to cuprates [27] but also quasi-1D systems with charge density waves, semiconductors and semimetals [28]. FT-STM of a 0.8% Fe covered surface of InAs revealed its quasiparticle dispersion, but its el-ph coupling is weak. In materials such as KCl, CsI, $SrTiO_3$ and RbCl, however, the el-ph coupling is up to two orders of magnitude stronger, while in $In_{1-x}Ga_xAs_yP_{1-y}$ it varies more than twice depending on the value of y [29]. Such systems at a low density of carries, or for very weak interactions between carriers, can be studied with our method.

As an example of its capabilities, we use IMA to generate results for a problem whose study by DMC is not feasible due to enormous CPU costs. We consider a case where there is no bare disorder, but the el-ph coupling varies randomly, $\lambda_i = g_i^2/(2dt\Omega) \in [0.9, 1.1]$ inside a finite region embedded in an infinite system with $\lambda = 1$. We consider the case of random el-ph coupling without on-site disorder because i) it demonstrates the usefulness of our method in a less familiar situation, and ii) it is relevant for studies like of ref. [7], where such inhomogeneous el-ph coupling is believed to exist.

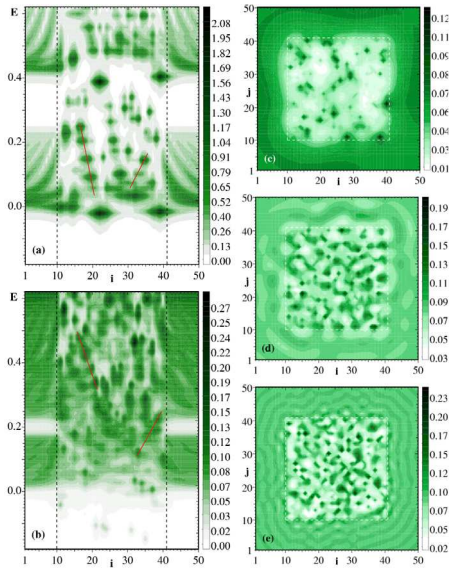

Fig. 4: (Color online) (a) 1D LDOS $A(i,E)$. The polaron band and part of the second bound-state band are shown. The vertical dashed lines mark the edges of the disordered region. The slanted lines suggest that some features' location changes with energy. (b) Analog of (a) for a 2D sample. The plot shows $A(i, j = 25, \omega)$ *vs.* i; (c),(d),(e) show the 2D $A(i,j,E)$ *vs.* i,j for $E = 0, 0.25$ and 0.5, respectively. In all plots the energy E is measured from the GS polaron energy of the surrounding uniform system with $\lambda = 1$, $\Omega = 0.5t, t = 1$.

Figures 4(a),(b) show clear evidence of nonlocal response, as some features change their spatial location with the energy (the slanted lines track a few such cases). This is more clear in 1D; in 2D some shifts are perpendicular to the direction shown. The LDOS maps of figs. 4(c)–(e) illustrate the retarded nature of the solution, with different looking LDOS inside the disordered region at different energies. There are no obvious correlations between these LDOS maps, in particular no common patterns that could be used to identify either a very large or very small local g_j. Our results also reproduce the expected Friedel-like oscillations in the surrounding region of uniform medium.

In ref. [7], the Fourier transform analysis of the LDOS maps assumes, as is usually done, that peaks occur at momenta $\mathbf{k}$ where the quasiparticles scatter most strongly at that energy. This fact can be used to extract the quasiparticle dispersion in the clean system, see also ref. [5]. However, in the absence of impurities, $\hat{V}_d = 0$, it is not clear how this scattering occurs. IMA reveals that it is due to the additional, el-ph induced potential $v(j,\omega)$. If this is true, FT of LDOS maps like those of figs. 4(c)–(e) should reveal the same phenomenology. Note that here we use nearest-neighbor hopping for the free electron, not the dispersion appropriate for a free quasiparticle in a clean d-wave superconductor, but this should not influence the general analysis. Moreover, IMA allows for straightforward generalization of the free particle dispersion.

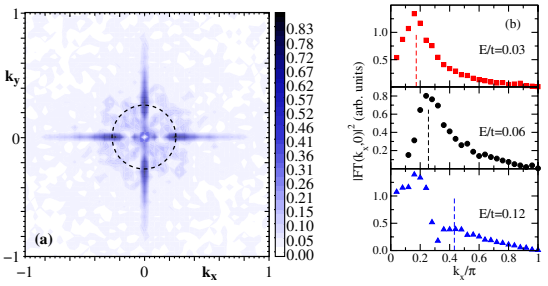

Fig. 5: (Color online) (a) Fourier transform of the 2D LDOS map at energy $E = 0.06t$ above the bulk GS ($\lambda = 1$, $\Omega = 0.5t$). (b) Same for $k_y = 0$ and $E/t = 0.03, 0.06, 0.12$. The lines show predicted scattering $\mathbf{k}_s$ vectors. For more details, see text.

In fig. 5(a) we show the average FT of 200 LDOS maps like those of fig. 4(c), but for disordered areas of 50×50 sites and at an energy $E = 0.06t$ above the bulk polaron GS. A large peak at $\mathbf{k} = 0$ peak was removed for clarity. As $E \to 0$, the bulk polaron dispersion $E(\mathbf{k}) = -2t^*(\cos k_x + \cos k_y - 2) \approx \frac{\hbar^2 \mathbf{k}^2}{2m^*}$, so we expect signal up to a $k_s = 2\sqrt{\frac{2m^*E}{\hbar^2}}$ when $\mathbf{k} \to -\mathbf{k}$ scattering occurs. For the parameters used here, the effective polaron mass is $m^*/m = t/t^* = 1.86$. The dashed line in fig. 5(a) shows k_s, in good agreement with the location of the FT maxima. This is revealed more clearly in fig. 5(b). (The second peak visible at higher E may be due to inelastic scattering between the first and second polaron bands, but this needs further study.) The good agreement proves that indeed it is the polaron of mass $m*$, not the bare particle of mass m, that is scattered. It also shows that even in the presence of such significant inhomogeneity, the polaron maintains its character. Our results are the first to provide a theoretical basis for FT analysis in such systems.

Because IMA is extremely efficient (LDOS maps like fig. 4(c) take ≈ 50 s on a desktop) one can now easily study very large samples with disorder in the on-site potential, the el-ph coupling and phonon energy, in any dimension, to reveal the effects of each kind of disorder and possible "interferences". For instance, it is possible that in the right circumstances, inhomogeneities of different origin may cancel out each others effects. Such studies are already under way [30]. Generalizations to other bare *qp* dispersions, to multiple phonon modes or to el-ph coupling dependent on the phonon momentum, where the bulk MA solutions are already known [18], are also straightforward.

In conclusion, IMA is an accurate, controllable and efficient method to study the effects of disorder on polarons.

* * *

Work supported by NSERC and CIFAR (MB), RFBR 07-02-0067a (ASM), and Grant-in-Aids No. 21244053, No. 19048008, No. 17105002, No. 19048015, and NAREGI Japan (NN).

REFERENCES

[1] Dagotto E., Hotta T. and Moreo A., *Phys. Rep.*, **344** (2001) 1.
[2] Millis A. J., *Phys. Rev. B*, **53** (1996) 8434; Perebeinos V. and Allen P. B., *Phys. Rev. Lett.*, **85** (2000) 5178.
[3] Uehara M. *et al.*, *Nature*, **399** (1999) 560.
[4] Motome Y., Furukawa N. and Nagaosa N., *Phys. Rev. Lett.*, **91** (2003) 167204.
[5] Pan S. H. *et al.*, *Nature*, **413** (2001) 282.
[6] Gunnarsson O. and Rösch O., *J. Phys.: Condens. Matter*, **20** (2008) 043201.
[7] Lee J. *et al.*, *Nature*, **442** (2006) 546.
[8] Matsui H. *et al.*, *Phys. Rev. Lett.*, **100** (2008) 126601.
[9] Borsenberger P. M. and Weiss D. S., *Organic Photoreceptors for Xerography* (Dekker, New York) 1998.
[10] Horowitz G. and Delannoy P., *J. Appl. Phys.*, **70** (1991) 469.
[11] Mishchenko A. S. *et al.*, *Phys. Rev. B*, **79** (2009) 180301.
[12] Hague J. P., Kornilovitch P. E. and Alexandrov A. S., *Phys. Rev. B*, **78** (2008) 092302.
[13] Pavlenko N. and Kopp T., *J. Phys.: Condens. Matter*, **20** (2008) 395203.
[14] Shinozuka Y. and Toyozawa Y., *J. Phys. Soc. Jpn.*, **46** (1979) 505.
[15] Balatsky A. V. and Zhu J.-X., *Phys. Rev. B*, **74** (2006) 094517.
[16] Bronold F. X. and Fehske H., *Phys. Rev. B*, **66** (2002) 073102; Bronold F. X., Alvermann A. and Fehske H., *Philos. Mag.*, **84** (2004) 673.
[17] Berciu M., *Phys. Rev. Lett.*, **97** (2006) 036402; Goodvin G. L., Berciu M. and Sawatzky G. A., *Phys. Rev. B*, **74** (2006) 245104.
[18] Covaci L. and Berciu M., *EPL*, **80** (2007) 67001; *Phys. Rev. Lett.*, **100** (2008) 256405; Goodvin G. L. and Berciu M., *Phys. Rev. B*, **78** (2008) 235120.
[19] Berciu M., *Phys. Rev. Lett.*, **98** (2007) 209702; Berciu M. and Goodvin G. L., *Phys. Rev. B*, **76** (2007) 165109.
[20] Mishchenko A. S. *et al.*, *Phys. Rev. B*, **62** (2000) 6317; Mishchenko A. S., *Phys. Usp.*, **48** (2005) 887.
[21] Barisic O. S., *Phys. Rev. Lett.*, **98** (2007) 209701.
[22] Goodvin G. L., Covaci L. and Berciu M., *Phys. Rev. Lett.*, **103** (2009) 176402.
[23] Bonca J., Trugman S. A. and Batistic I., *Phys. Rev. B*, **60** (1999) 1633.
[24] Burovski E., Fehske H. and Mishchenko A. S., *Phys. Rev. Lett.*, **101** (2008) 116403.
[25] Macridin A. *et al.*, *Phys. Rev. B*, **69** (2004) 245111.
[26] Sprunger P. T. *et al.*, *Science*, **275** (1997) 1764.
[27] McElroy K. *et al.*, *Nature*, **422** (2003) 592.
[28] Brun C. *et al.*, *Phys. Rev. B*, **80** (2009) 045423; Sagisaka K. and Fujita D., *Phys. Rev. B*, **72** (2005) 235327; Morgenstern M. *et al.*, *Phys. Rev. Lett.*, **89** (2002) 136806; Vonau F. *et al.*, *Phys. Rev. B*, **69** (2004) 081305.
[29] Devreese J. T., *Polarons in Ionic Crystals and Polar Semiconductors* (North-Holland, Amsterdam) 1972.
[30] Ebrahimnejad H. *et al.*, unpublished.